

Studies of PDFs, GPDs and TMDs at the JLab 12 GeV Upgrade

V. D. BURKERT

Jefferson Lab - Newport News, VA 23606, USA

ricevuto il 24 Novembre 2011; approvato il 6 Dicembre 2011
pubblicato online il 7 Marzo 2012

Summary. — This talk is intended as a brief overview of the Jefferson Lab program to study the multi-dimensional structure of the nucleon in coordinate and momentum space. The experimental program is very extensive and, given the limited space available, only selective samples can be discussed.

PACS 13.60.-r – Photon and charged-lepton interactions with hadrons.

PACS 13.60.Hb – Total and inclusive crosssections (including deep-inelastic processes).

PACS 13.60.Fz – Elastic and Compton scattering.

PACS 13.60.Le – Meson production.

1. – Introduction

The challenge of understanding nucleon structure remains after more than five decades of experimental scrutiny. From the first measurements of elastic form factors to the accurate determination of parton distributions through deep inelastic scattering (DIS), the experiments have vastly improved in statistics and systematic uncertainty. It was realized in recent years that the parton distribution functions represent special cases of a more general, and much more powerful way of characterizing the structure of the nucleon, the generalized parton distributions (GPDs) [1] and the transverse momentum distributions (TMDs) [2,3].

The GPDs describe the simultaneous distribution of particles with respect to both transverse coordinate and longitudinal momentum. In addition to the information about the spatial density and parton momentum density, these functions reveal the correlation of the spatial and momentum distributions. GPDs also allow us to quantify how the orbital motion of quarks in the nucleon contributes to the nucleon spin [4] —a question of crucial importance to our understanding of the dynamics underlying nucleon structure. The mapping of the nucleon GPDs through deeply virtual exclusive processes such as DVCS, are key objectives of nuclear physics of the next decade.

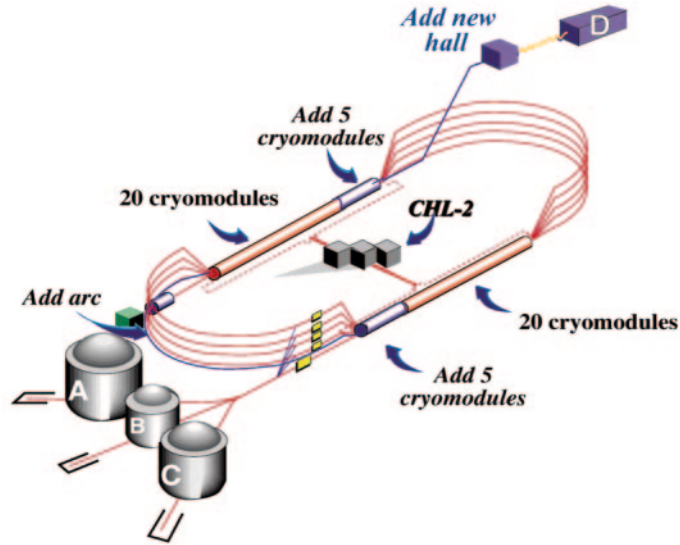


Fig. 1. – The Jefferson Lab continuous electron beam accelerator facility showing the components needed for the 12 GeV upgrade.

TMDs provide information that is complementary to GPDs, and access the quark spin distributions in 3D momentum space. TMDs can be accessed through semi-inclusive deeply inelastic scattering (SIDIS) on unpolarized and polarized nucleon targets.

The study of longitudinal parton distribution function (PDFs) has been a focus of hadron physics for several decades resulting in precise knowledge of the unpolarized quark distributions. The polarized parton distribution functions have not been determined nearly as well and much more precise data especially on polarized structure function $g_1(x, Q^2)$ are needed to address open issues such as their Q^2 evolution to determine the polarized gluon density.

These avenues of research can be explored using the 12 GeV cw beam of the JLab upgrade with much higher precision than has been possible before. Also, the high luminosity will enable probing the very high x regime, where a single quark carries 80% or more of the proton's total momentum. In sect. 2 a brief overview is given of the upgrade of the JLab accelerator to 12 GeV and of the experimental equipment that is currently under construction or has been proposed. In sect. 3 I discuss some of the improvements that can be achieved on the longitudinal quark and gluon distributions, and in sects. 4 and 5 I discuss experimental aspects of the GPD and TMD programs.

2. – The electron accelerator and the 12 GeV experimental equipment

The electron accelerator is shown schematically in fig. 1. The two linear accelerators are based on superconducting rf technology. Spin polarized electrons are generated in the gun and pre-accelerated to 50 MeV in the injector shown at the upper left end of the racetrack. They are then boosted in the north linac to about 600 MeV. They are then bent by 180 degrees and injected into the south linac to be accelerated to up to 1200 MeV. This is repeated four more times when the final energy of 6000 MeV is reached. For the energy upgrade five accelerating cryomodules with four times higher gradients per unit



Fig. 2. – Experimental equipment to support the multi-dimensional nucleon structure program at the JLab 12 GeV upgrade.

length are added to both linacs to reach a maximum energy at the existing end stations of nearly 11 GeV. One arc and one more path through the north linac are added to accelerate the beam to 12 GeV and transport it to the new Hall D.

Major equipment upgrades are planned to support a broad program of nuclear and nucleon physics and to study the quark-gluon dynamics and multi-dimensional structure of the nucleon. The two top panels in fig. 2 show the baseline equipment that is currently under construction. The left panel shows the new CLAS12 large acceptance spectrometer, the panel on the right shows the spectrometer pair in Hall C including the new SHMS spectrometer. The CLAS12 and SHMS are projected to be available for physics in 2015. The central graph at the bottom is the concept of the large acceptance RICH detector to upgrade CLAS12 for improved charged particle identification capabilities. The panel on the left shows the proposed SBS spectrometer in Hall A, and on the right the concept of a solenoid spectrometer. In addition to the new equipment that is under construction a highly polarized electron gun and several targets are available using polarized NH_3 , ND_3 , HD, butanol, and ^3He .

3. – Inclusive structure functions and parton distributions

Polarized and unpolarized structure functions of the nucleon offer unique insights into the two defining features of QCD — asymptotic freedom at small distances, and confinement and non-perturbative effects at large distance scales. After more than three decades of measurements at many accelerator facilities worldwide, a truly impressive amount of data has been collected, covering several orders of magnitude in both kinematic variables x and Q^2 . One uncharted area is the behavior of the structure functions in

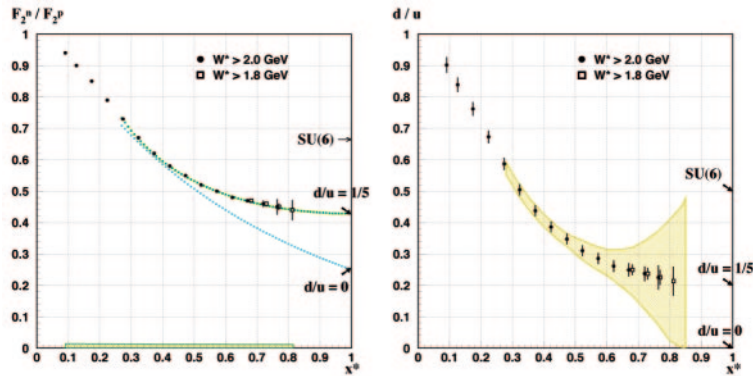


Fig. 3. – Projected data for the ratio F_{2n}^n/F_{2p}^p and $d(x)u(x)$ from experiment [9]. The systematic errors are given by the area near the horizontal axis. The yellow band shows the uncertainty of current data due to uncertainties in the nuclear corrections.

the extreme kinematic limit $x \rightarrow 1$ where contributions from the virtual sea of quark-antiquark pairs are suppressed, making this region simpler to model, and pQCD can make absolute predictions. However, the large x domain is hard to reach because cross sections are kinematically suppressed, the parton distributions are small and final state interactions (partonic or hadronic) are large. First forays into the large x domain became possible at energies of 5–6 GeV [5–8]. The interest triggered by these first results and the necessity to extend the program to larger x provided one of the cornerstone of the JLab 12 GeV upgrade physics program. The unpolarized structure function $F_{2p}(x)$ has been mapped out in a large range of x leading to precise knowledge of the quark distribution $u(x)$. The corresponding structure function $F_{2n}(x)$ is well measured only for $x < 0.5$ as nuclear corrections, when using deuterium as a target, become large at large x . As a consequence, the d -quark distribution is much less well determined at large values of x . This is one of the open problems in inclusive DIS.

A new technique has recently been shown at CLAS to be very effective in reducing the nuclear corrections [8]. The experiment used a radial TPC with GEM readout as detector for the low-energy spectator proton in the reaction $en(p_s) \rightarrow ep_s X$. Measurement of the spectator proton for momenta as low as 70 MeV/ c and at large angles minimizes the poorly known nuclear corrections at large x . The techniques will be used at 12 GeV to accurately determine the ratio $d(x)/u(x)$ to much larger x values that it is known today [9]. Another experiment employs the ratio method [10] using the mirror nuclei ${}^3\text{He}$ and a ${}^3\text{H}$ as targets where nuclear effects are expected to cancel. Figure 3 shows the projected data for $F_{2n}^n(x)/F_{2p}^p(x)$ and $d(x)/u(x)$ using the spectator tagging method. A dramatic improvement can be achieved at large x .

Precise information is also lacking for the spin structure function $g_1(x, Q^2)$ and the helicity asymmetry $A_1(x)$ at large values of x . Several experiments [11–13] will study polarized parton distributions at large x using polarized NH_3 , ND_3 , and ${}^3\text{He}$ as target material. Examples of the improvement expected for the polarized d -quark density and the asymmetry of the polarized sea are shown in fig. 4.

Parton distribution functions are extracted from experimental data in global analysis that make use of all available data. The limited information available for the polarized structure function $g_1(x, Q^2)$ has as a consequence that the polarized gluon density $\Delta G(x)$

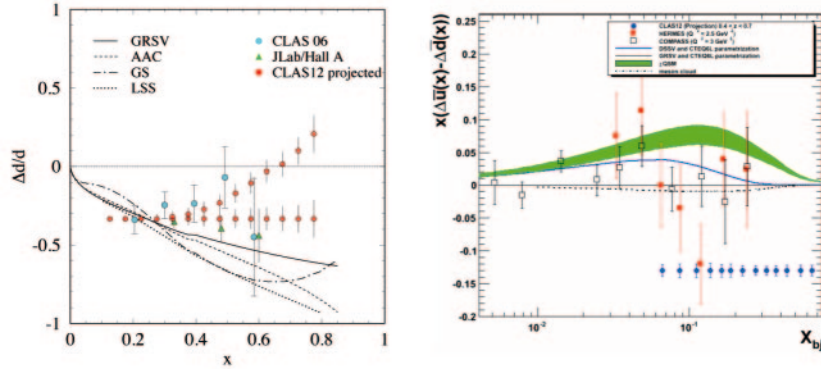


Fig. 4. – Left panel: Expected results for $(\Delta d + \Delta \bar{d})/(d + \bar{d})$. The central values of the data are following two curves to demonstrate how the two categories of predictions, namely the ones that predict $\Delta d/d$ stays negative and the ones predicting $\Delta d/d \rightarrow 1$ when $x \rightarrow 1$. The right panel shows the expected uncertainties for the asymmetry of the polarized sea.

is the least constrained of the parton distribution function. The precision of the expected data on $g_1(x, Q^2)$ at 12 GeV provides a model-independent way to extract $\Delta G(x)$ through the Q^2 dependence of $g_1(x, Q^2)$ measured in a large interval of Q^2 . Projection of one analysis [14] are shown in fig. 5. JLab data at lower energies had already visible impact on ΔG at large x . The improvement from the 12 GeV upgrade is even more significant and also impacts $\Delta G(x)$ at lower x . The projected data will not only reduce the error band on ΔG , but will likely allow a more detailed modeling of its x -dependence.

4. – Generalized parton distributions and DVCS

At intermediate and lower energies, deeply virtual Compton scattering (DVCS) is most suitable for charting the twist-2 vector GPDFs H, E and the axial GPDF \tilde{H} . They

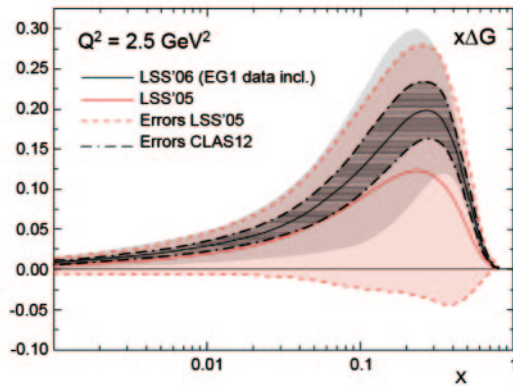


Fig. 5. – Expected uncertainties for $x\Delta G$. The black solid curve shows the central value of the present analysis that includes lower energy JLab data. The dark shaded area is the projected uncertainty for ΔG using the expected data from experiment [11].

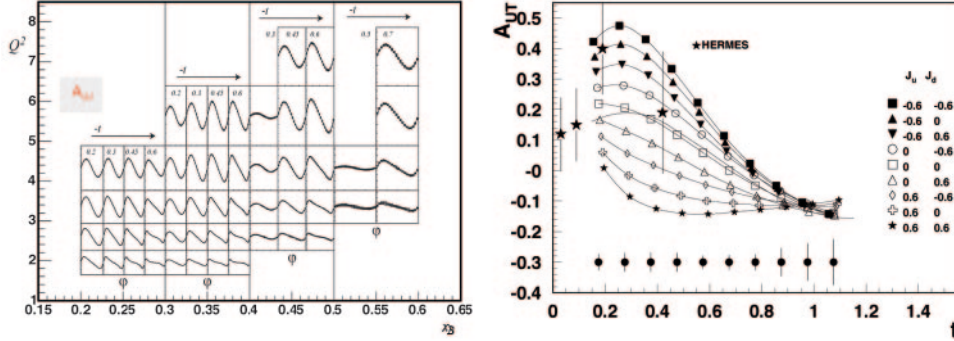


Fig. 6. – Projected data for the beam spin asymmetry A_{LU} (left panel) and for the transverse target asymmetry (right panel) for the DVCS-BH interference for experiment [24]. The t dependence of A_{UT} is shown for a single bin in Q^2 and x .

provide access to nucleon imaging in 2 and 3 dimensions and opens up new insights into the complex dynamics of the nucleon. Moreover, GPDs carry information of more global nature. The nucleon matrix element of the energy-momentum tensor contains 3 scalar form factors $J(t)$, $M_2(t)$, $d_1(t)$, that encode information on the transverse density of angular momentum, mass, and forces, respectively. They appear as moments of the vector GPDs [15], thus offering prospects for accessing gravitational form factors through the detailed mapping of GPDs. For example, the quark angular momentum density in impact parameter space can be obtained from a Fourier transformation of $J(t)$ as expressed through the relation $J^q(t) = \int_{-1}^{+1} dx x [H^q(x, \xi, t) + E^q(x, \xi, t)]$.

For the determination of GPDs, measurement of polarization observables is crucial. The beam helicity-dependent cross section asymmetry is given in leading twist as $A_{LU} \approx \sin \phi [F_1(t)H + \xi(F_1 + F_2)\tilde{H}]d\phi$, where ϕ is the azimuthal angle between the electron scattering plane and the hadronic plane. The kinematically suppressed term with GPD E is omitted. A_{LU} is mostly sensitive to the GPD $H(x = \xi, \xi, t)$.

The target asymmetry $A_{UL} = \Delta\sigma_{UL}/2\sigma$ accesses the same GPDs but is more sensitive to \tilde{H} , while H is kinematically unfavored, although at not too small values of ξ , H and \tilde{H} both contribute, and the combined analysis of A_{LU} and A_{UL} enables the separation of GPD $H(x = \xi, \xi, t)$ and $\tilde{H}(x = \xi, \xi, t)$. Using a transversely polarized target the asymmetry $A_{UT} \approx \cos \phi \sin(\phi - \phi_s) [t/4M^2(F_2H - F_1E)]$ can be measured, where ϕ_s is the azimuthal angle of the target polarization vector relative to the electron scattering plane. A_{UT} depends in leading order on GPD E .

The first DVCS experiments carried out at JLab [16-19] and DESY [20] showed promising results in terms of the dominance of the leading twist “handbag” mechanism, and the applicability to probe GPDs. Information directly related to GPDs has recently been extracted from JLab and Hermes data in several independent analysis [21-23]

The 12 GeV upgrade offers much improved possibilities for accessing GPDs. Experiments will measure cross sections and beam spin asymmetry on protons [24, 25] and neutrons [26]. Figure 6 shows the expected statistical precision of the beam asymmetry in the full kinematic range available. Using polarized targets one measures the target spin asymmetries with high precision [24]. The right panel in fig. 6 shows the expected statistical accuracy for one kinematics bin of the proton transverse target asymmetry. A measurement of all 3 asymmetries will enable the separation of GPDs H , \tilde{H} and E at

TABLE I. – *Leading-twist transverse momentum-dependent distribution functions. U, L, and T stand for transitions of unpolarized, longitudinally polarized, and transversely polarized nucleons (rows) to corresponding quarks (columns).*

N/q	U	L	T
U	\mathbf{f}_1		h_1^\perp
L		\mathbf{g}_1	h_{1L}^\perp
T	f_{1T}^\perp		\mathbf{h}_1 h_{1T}^\perp

the above specified kinematics. A Fourier transformation of GPD $H(t)$ allows access to the quark distribution in transverse impact parameter space.

5. – Semi-inclusive DIS and TMDs

SIDIS processes, where the leading, high momentum hadron is detected in coincidence with the scattered lepton, are used for “flavor tagging” of quarks to select contributions from different quark species. Currently, the emphasis is to study SIDIS processes that encode information on the transverse momentum distributions of quarks, information that is not otherwise accessible. For example, azimuthal distributions of final state particles in SIDIS provide access to the orbital motion of quarks and play an important role in the study of TMDs of quarks in the nucleon.

TMD distributions describe transitions of a nucleon with one polarization in the initial state to a quark with another polarization in the final state. The diagonal elements of table I are the momentum, longitudinal and transverse spin distributions of partons, and represent well-known parton distribution functions related to the square of the leading-twist, light-cone wave functions. Off-diagonal elements require non-zero orbital angular

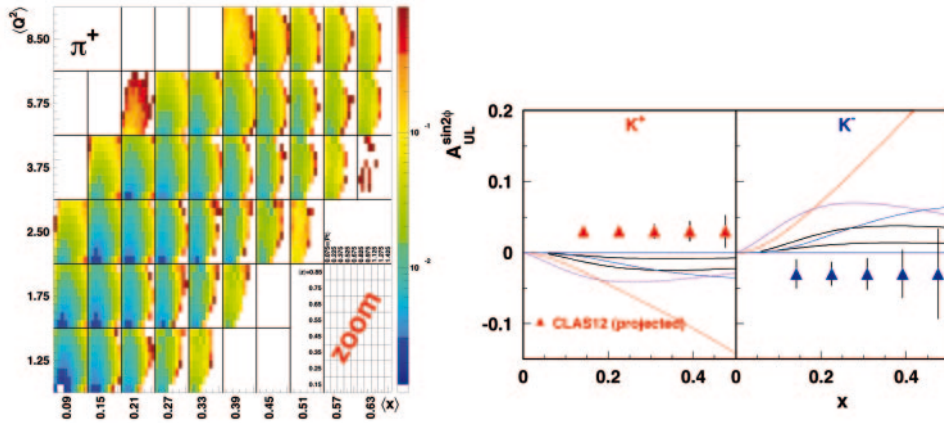


Fig. 7. – Left panel: Kinematic coverage and projected uncertainties of the 4-dimensional π^+ yield in Q^2 , x , z , and p_T . The color code shows the relative errors in each bin. Right panel: Projected x -dependence of the polarized spin target asymmetry at 11 GeV with CLAS12 for kaons for one bin in Q^2 , z , p_T .

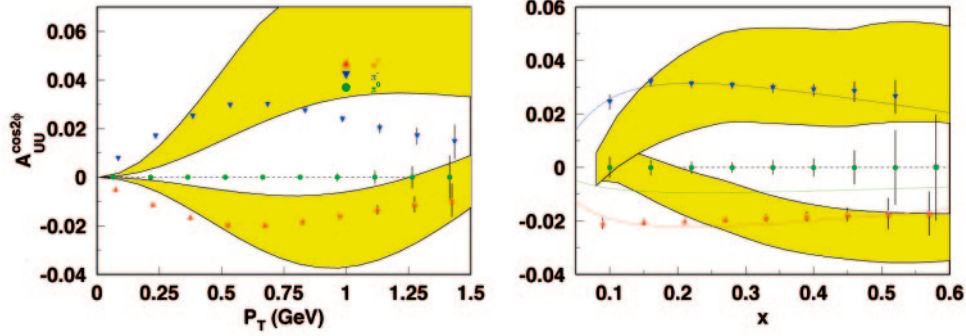


Fig. 8. – The $\cos 2\phi$ moment (Boer-Mulders asymmetry) for pions as a function of Q^2 and P_T for $Q^2 > 2 \text{ GeV}^2$ (right) with CLAS12 at 11 GeV from 2000 hours of running. Values are calculated assuming $H_1^{\perp u \rightarrow \pi^+} = -H_1^{\perp u \rightarrow \pi^-}$. Only statistical uncertainties are shown. The yellow band between the two curves indicated the range of two model predictions.

momentum and are related to the wave function overlap of $L = 0$ and $L = 1$ Fock states of the nucleon. The chiral-even distributions f_{1T}^{\perp} and g_{1T} are the imaginary parts of the corresponding interference terms, and the chiral-odd h_1^{\perp} and h_{1L} are the real parts. The TMDs f_{1T}^{\perp} and h_1^{\perp} , which are related to the imaginary part of the interference of wave functions for different orbital momentum states and are known as the Sivers and Boer-Mulders functions. They describe unpolarized quarks in the transversely polarized nucleon and transversely polarized quarks in the unpolarized nucleon respectively. The most simple mechanism that can lead to a Boer-Mulders function is a correlation between the spin of the quarks and their orbital angular momentum. In combination with a final state interaction that is on average attractive, already a measurement of the sign of the Boer-Mulders function, would thus reveal the correlation between orbital angular momentum and spin of the quarks. Similar to the extraction of GPDs, TMD studies will greatly benefit from the higher energy and luminosity available at 12 GeV. A comprehensive program is in preparation at JLab to study the new distribution functions. The

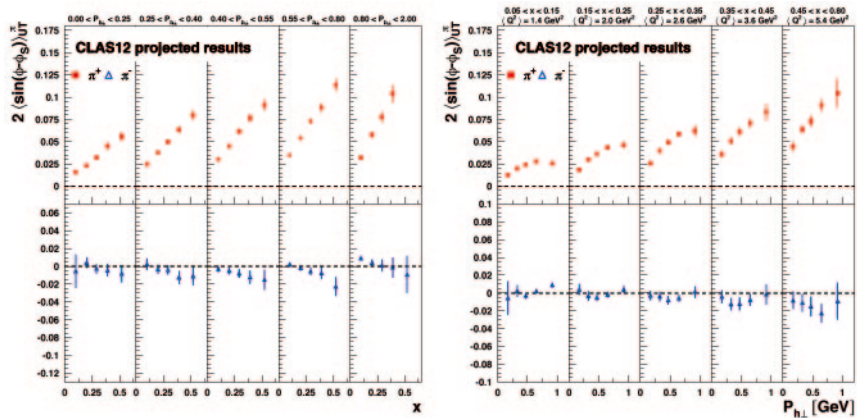


Fig. 9. – Projected data for the Sivers function *vs.* x for different transverse momentum bins (left panel) and *vs.* p_T for different x bins.

main focus is the measurement of SIDIS processes in the full phase space available in Q^2 , x , z and p_T . The left panel in fig. 7 shows the phase space coverage and statistical precision expected for semi-inclusive π^+ production.

Several experiments will study the Boer-Mulders asymmetry [27,28]. Examples are presented in fig. 8. Several experiments will study the Sivers asymmetries on polarized hydrogen [29] and on polarized ^3He [30]. Examples of kinematic dependences are shown in fig. 9. Although pions have been the main focus of SIDIS experiment in the past, the K^+ and K^- channels have recently emerged as of high interest as well. Hermes results show unexpectedly large Boer-Mulders asymmetries for kaons compared to pions, and the opposite signs for K^- and π^- . Several experiments [29,31-33] will measure semi-inclusive processes for kaon productions. With the excellent particle identification and high luminosity expected for CLAS12, these puzzling issues can be addressed efficiently. The right panel in fig. 7 shows the statistical precision for K^+ and K^- production on a polarized hydrogen target in one kinematic bin in Q^2 , z , and p_T .

6. – Conclusions

The JLab 12 GeV energy upgrade and the planned new experimental equipment are well matched to an exciting scientific program aimed at studies of the complex nucleon structure. The longitudinal and transverse momentum dependent parton distribution functions are critical components in this program. GPDs and TMDs provide fundamentally new insights into the complex internal dynamics of the nucleon. As GPDs, TMDs, and PDFs represent different projections of a multi-dimensional Wigner function, the combined measurements and global analyses of deeply exclusive, semi-inclusive, and inclusive processes will bring us a major step forward in the quest to unravel the nucleon's internal dynamics. The high precision afforded by the high luminosity and the large acceptance detectors, and the development of novel techniques will enable the exploration of phase space domains with extreme conditions that could not be studied before. The CLAS12 detector will be at the core of this exciting program.

* * *

This work was supported in part by the U.S. Department of Energy and the National Science Foundation, the French Commissariat à l'Énergie Atomique, the Italian Istituto Nazionale di Fisica Nucleare, the Korea Research Foundation, and a research grant of the Russian Federation. The Jefferson Science Associates, LLC, operates Jefferson Lab under contract DE-AC05-06OR23177.

REFERENCES

- [1] MUELLER D. *et al.*, *Fortsch. Phys.*, **42** (1994) 101.
- [2] MULDER P. J. and TANGEMAN R. D., *Nucl. Phys. B*, **461** (1996) 197.
- [3] BOER D. and MULDER P. J., *Phys. Rev. D*, **57** (1998) 5780.
- [4] BURKARDT M., *Int. J. Mod. Phys. A*, **18** (2003) 173.
- [5] ZHENG X. *et al.*, *Phys. Rev. C*, **70** (2004) 065207.
- [6] DHARMAWARDANE V. *et al.*, *Phys. Lett. B*, **641** (2006) 11.
- [7] BOSTED P. *et al.*, *Phys. Rev. C*, **75** (2007) 035203.
- [8] BAILLIE N. *et al.*, arXiv:1110.2770 (2011).
- [9] BUELTMAN S. *et al.*, JLAB EXPERIMENT E12-10-113, 2006.
- [10] PETRATOS G. *et al.*, JLAB EXPERIMENT E12-10-103, 2010.

- [11] KUHN S. *et al.*, JLAB EXPERIMENT E12-06-109, 2006.
- [12] MEZIANI Z.-E. *et al.*, JLAB EXPERIMENT E12-06-110, 2006.
- [13] CATES G. *et al.*, JLAB EXPERIMENT E12-06-122, 2006.
- [14] LEADER E., SIDOROV S. and STAMENOV D., *Phys. Rev. D*, **75** (2007) 074027.
- [15] GOEKE K. *et al.*, *Phys. Rev. D*, **75** (2007) 094021.
- [16] STEPANYAN S. *et al.*, *Phys. Rev. Lett.*, **87** (2001) 182002.
- [17] GIROD F. X. *et al.*, *Phys. Rev. Lett.*, **100** (2008) 162002.
- [18] MUNOZ-CAMACHO C. *et al.*, *Phys. Rev. Lett.*, **97** (2006) 262002.
- [19] CHEN S. *et al.*, *Phys. Rev. Lett.*, **97** (2006) 072002.
- [20] AIRAPETIAN A. *et al.*, *Phys. Rev. Lett.*, **87** (2001) 182001.
- [21] KUMERICKI K. and MUELLER D., *Nucl. Phys. B*, **841** (2010) 1.
- [22] GUIDAL M., *Phys. Lett. B*, **693** (2010) 17.
- [23] MOUTARDE H., *Phys. Rev. D*, **79** (2009) 094021.
- [24] SABATIE F. *et al.*, JLAB EXPERIMENT E12-06-119, 2006.
- [25] HYDE C. *et al.*, JLAB EXPERIMENT E12-10-114, 2010.
- [26] NICCOLAI S. *et al.*, JLAB EXPERIMENT E12-11-003, 2011.
- [27] AVAKIAN H. *et al.*, JLAB EXPERIMENT E12-07-107, 2007.
- [28] ENT R. *et al.*, JLAB EXPERIMENT E12-09-017, 2009.
- [29] CONTALBRIGO M. *et al.*, JLAB EXPERIMENT C12-11-111, 2011.
- [30] GAO H. *et al.*, JLAB EXPERIMENT E12-11-006, 2011.
- [31] WOJSEKOWSKI B. *et al.*, JLAB EXPERIMENT E12-09-018, 2009.
- [32] AVAKIAN H. *et al.*, JLAB EXPERIMENT E12-09-007, 2009.
- [33] AVAKIAN H. *et al.*, JLAB EXPERIMENT E12-09-008, 2009.